Cancer Immunology, Immunotherapy (2019) 68:1287–1301
https://doi.org/10.1007/s00262-019-02361-5

ORIGINAL ARTICLE

Reduced CTL motility and activity in avascular tumor areas

Yoav Manaster[1] · Zohar Shipony[1] · Anat Hutzler[1] · Masha Kolesnikov[1] · Camila Avivi[2] · Bruria Shalmon[2] · Iris Barshack[2] · Michal J. Besser[3,4] · Tali Feferman[1] · Guy Shakhar[1]

Received: 10 January 2019 / Accepted: 16 June 2019 / Published online: 28 June 2019

Abstract

Patchy infiltration of tumors by cytotoxic T cells (CTLs) predicts poorer prognosis for cancer patients. The factors limiting intratumoral CTL dissemination, though, are poorly understood. To study CTL dissemination in tumors, we histologically examined human melanoma samples and used mice to image B16-OVA tumors infiltrated by OT-I CTLs using intravital two-photon microscopy. In patients, most CTLs concentrated around peripheral blood vessels, especially in poorly infiltrated tumors. In mice, OT-I CTLs had to cluster around tumor cells to efficiently kill them in a contact-and perforin-dependent manner and cytotoxicity was strictly antigen-specific. OT-I CTLs as well as non-specific CTLs concentrated around peripheral vessels, and cleared the tumor cells around them. This was also the case when CTLs were injected directly into the tumors. CTLs crawled rapidly only in areas within 50 µm of flowing blood vessels and transient occlusion of vessels immediately, though reversibly, stopped their migration. In vitro, oxygen depletion and blockade of oxidative phosphorylation also reduced CTL motility. Taken together, these results suggest that hypoxia limits CTL migration away from blood vessels, providing immune-privileged niches for tumor cells to survive. Normalizing intratumoral vasculature may thus synergize with tumor immunotherapy.

Keywords CTLs · Hypoxia · Cell motility · Tumor vasculature · Tumor immunotherapy · Intravital imaging

Abbreviations

ALP-red	Alkaline phosphatase red
CFP	Cyan fluorescent protein
DAB	3,3′-Diaminobenzidine
DIC	Differential interference contrast
FAS	First apoptosis signal
FasL	Fas ligand
FCCP	Carbonyl cyanide-4-(trifluoromethoxy) phenylhydrazone
HIF-1α	Hypoxia inducible factor 1 α
IRES	Internal ribosome entry site

Introduction

Cytotoxic T lymphocytes (CTLs) have long been recognized to be pivotal in limiting the development of immunogenic tumors. These cells can reject tumors when transferred to model animals [1], they recognize tumor-associated antigens in patients [2], and their presence within many tumors is a positive prognostic sign [3]. In accordance, in successful immunotherapies such as anti-CTLA4 and anti-PD-1, CTLs emerge as key effector cells [4], as clonal anti-tumor CD8 immune response and vigorous infiltration of tumors [5] predict tumor responsiveness.

CTLs can directly kill their antigen-specific targets by delivering cytolytic granules containing perforin and granzymes to their membranes [6], or by activating death receptors such as first apoptosis signal (FAS) [7], in both

Electronic supplementary material The online version of this article (https://doi.org/10.1007/s00262-019-02361-5) contains supplementary material, which is available to authorized users.

✉ Tali Feferman
tali.feferman@weizmann.ac.il

✉ Guy Shakhar
shakhar@weizmann.ac.il

[1] Department of Immunology, Weizmann Institute of Science, Wolfson Bldg., 234 Herzl St., 76100 Rehovot, Israel

[2] Department of Pathology, Sheba Medical Center, Derech Sheba 2, 52621 Ramat Gan, Israel

[3] Ella Institute, Sheba Medical Center, Derech Sheba 2, 52621 Ramat Gan, Israel

[4] Department of Human Microbiology and Immunology, Sackler Medical School, Tel-Aviv University, 35 Klachkin st, 6997801 Tel Aviv, Israel

cases usually triggering apoptotic cell death [8, 9]. CTLs can also induce tumor rejection indirectly, by releasing cytokines such as IFN-γ which recruit innate effector cells into the tumor [9, 10]. In such cases, bystander tumor cells, which do not present relevant antigens, can also be eliminated.

Going beyond the long-established predictive value of total numbers of infiltrating CTLs, later analyses have also examined their location within tumors. Favorable prognosis has been associated with more homogenous CTL distribution [11, 12]. It was not shown; however, how restricted distribution prevents tumor clearance and it remains unclear what factors limit CTL spread.

A likely environmental factor influencing intratumoral distribution of CTLs is the pattern and integrity of the blood vessels through which they enter the tumor. It has been reported that CD8 T cells tend to remain close to blood vessels [13] and a clinical study [12] confirmed the prognostic value of total CD8 T-cell counts in tumors and observed that a small minority of patients (~ 8%) whose $CD45^+$ leucocyte infiltrate extended through the tumors enjoyed a much better prognosis than patients whose leucocytes remained close to blood vessels (~ 60% vs. ~ 30% survival at 60 months). It is still unclear why the leucocytes stayed in the perivascular areas in most patients.

An attractive possibility is that hypoxia, prevalent in avascular tumor areas, plays a role. Indeed, many tumors contain hypoxic pockets because of inadequate vascularization, and lower intratumoral oxygen pressure is often a negative prognostic factor [14, 15]. Correspondingly, T-cell motility was shown to depend on high oxygen levels [16], as CD8 T cells can sense hypoxia through signaling pathways such hypoxia inducible factor 1 α (HIF-1α), and may be limited in their capacity to utilize glycolysis in the absence of oxygen [17]. Most revealingly, a recent study showed that intratumoral T cells avoid hypoxic tumor areas and that exposing mice to constantly high oxygen levels encourage intratumoral accumulation of CD8 T cells and greatly improve tumor rejection [18]. Taken together, these findings suggest that hypoxia may hinder CTL dissemination throughout tumors, worsening prognosis.

A powerful method to study the motility of CTLs within tumors is intravital two-photon microscopy [19]. Studies utilizing it have found that T cells can crawl at high speeds within tumors [20, 21], sometimes along blood vessels [22], but have not examined the influence of vascularity and rarely recorded instances of tumor cell killing [21].

Here, we examine histological data from clinical melanoma samples and dynamic data from a mouse tumor model to evaluate the causes and consequences of limited CTL distribution in tumors.

Materials and methods

Patients

Tumor samples were from 16 untreated patients diagnosed with melanoma who were awaiting immunotherapy at the Ella Institute at the Sheba Medical Center in Ramat Gan, Israel. The patients' mean age was 55.3, 10 were male, and 6 were female. Cutaneous melanoma lesions, representing early metastases, had been surgically removed from patients and their frozen samples were available at the archives of the Department of Pathology at Sheba.

Immunostaining of human melanoma samples

Formalin-fixed, paraffin-embedded tumor tissue sections were prepared at 4 μm thickness and had a mean diameter of 5.5 mm. Sections were warmed up to 60 °C for 1 h, deparaffinized in xylene, and rehydrated. The CD8 and CD31 double immunostaining was calibrated on a Benchmark XT staining module (Ventana Medical Systems Inc.). The slides were then processed in a fully automated protocol [23] and a cell conditioning 1 (CC1) Standard Benchmark XT pretreatment for antigen retrieval was selected. Samples were incubated for 44 min at 37 °C with anti-CD8 (recombinant monoclonal antibody 012, Diagnostic BioSystems) and anti-CD31 (M0823, Dako), both diluted 1:25. Detection was performed first with 3,3′-diaminobenzidine (DAB) for anti-CD31 and then with alkaline phosphatase red (ALP-red) for anti-CD8; both using ultraView Universal Detection kits. Counterstaining was performed with hematoxylin. After staining, slides were dehydrated in 70%, 95%, and 100% ethanol for 1 min each, cleared in xylene for 1 min, and mounted with Entellan. Reagents for sample preparation were from Ventana.

Histological image analysis

Double-stained sections were viewed with a light microscope at a magnification of 400× and analyzed. Suitable digital images were captured using bright-field digital slide scanner (3DHISTECH Ltd,) with the Panoramic Viewer software at 0.33 μm/pixel. Analysis was carried out using the ImageJ software (version 1.38). DAB and ALP-red staining was separated using color deconvolution, and $CD31^+$ blood vessels and $CD8^+$ cells were segmented accordingly (Fig. S1). To define perivascular areas around dense concentrations of CD31, we used a blurring convolution matrix on $CD31^+$ pixels, followed by thresholding. To estimate the number of $CD8^+$ cells, the total $CD8^+$ area was divided by the average measured cross-sectional area of a

$CD8^+$ cell. $CD8^+$ cell densities in vascular and avascular areas were calculated for their respective areas (Fig. S1). To study the regional distribution of $CD8^+$ cells, we defined the outermost area of each tumor section as "peripheral" (Fig. S1F), and compared the concentrations of $CD8^+$ cells around peripheral and central blood vessels. The cross-sectional areas (*A*) and $CD8^+$ T-cell counts (*C*) of vascular regions (*v*) including peripheral vascular (pv), and deep vascular (dv) regions, and of avascular (av) and total (*t*) regions, were determined (Table S1). These measurements were used to calculate the $CD8^+$ cell densities (*D*) in each area: ($Dv = Cv/Av$, $Dpv = Cpv/Apv$, $Ddv = Cdv/Adv$, $Dav = Cav/Aav$, $Dt = Ct/At$). The relative $CD8^+$ cell densities (Fig. 1d) were calculated for each region as Dpv/Dt, Ddv/Dt, and Dav/Dt). The ratio of $CD8^+$ cell densities in vascular and avascular areas (Dv/Dav) and the log10 of total $CD8^+$ cell density (Dt) were calculated, as shown in Fig. 1e.

Mouse strains

C57BL/6 mice and several transgenic mouse strains were used. These were: mice expressing cyan fluorescent protein (CFP) under the β-actin promoter [B6.129(ICR)-Tg(ACTB-ECFP)CK6Nagy/J], mice expressing GFP under the human ubiquitin C promoter [C57BL/6-Tg(UBC-EGFP)30Scha/J], and TCR-transgenic OT-I mice, whose TCR recognized the peptide SIINFEKL from the OVA protein presented on H2 ^{Kb} MHC-I molecules [C57BL/6-Tg(TcraTcrb)1100Mjb/J], and mice deficient in Fas Ligand (FasL) or in perforin, thoroughly backcrossed to the C57BL/6 [24], were crossed with TCR-transgenic OT-I mice to create OT-I $FasL^{-/-}$ and OT-I $Perforin^{-/-}$ mice.

Tumor cells

Cells from the B16a melanoma line [25], which are slow to express melanin in vivo, were retrovirally transduced with a plasmid provided by the Forchheimer repository at the Weizmann Institute. OVA-IRES-tdTomato and the control tdTomatto constructs were expressed on the pBABE PURO retroviral vector, and the OVA-IRES-GFP constructs were expressed on the retroviral pMMP plasmid. Cells were sorted using a FACS Aria (Becton–Dickinson) for high fluorescence. After 4–6 sorting and culturing cycles, cells were grown in limiting dilution conditions and single clones were selected, aliquoted, and frozen.

Tumor inoculation and follow-up

Two million tumor cells were re-suspended in 60 µl of PBS and injected intradermally into the footpad or to the flank skin. A caliper was used to measure the thickness of the footpad or to measure the width and length of the tumor, and tumor areas were calculated by multiplying those measurements.

T-cell culture and adoptive transfer

GFP or CFP-labeled splenocytes from wild-type or OT-I mice were harvested from the spleen and LNs. To isolate polyclonal CD8 T cells, wild-type splenocytes were sorted with an EasySep™ CD8 negative magnetic isolation kit (STEMCELL technologies). To produce Ag-specific CTLs, OT-I cells were incubated in RPMI containing the SIINFEKL peptide (50 µg/ml) for 2 h, re-suspended in complete RPMI medium, and 3 days later purged of dead cells using ficoll gradient centrifugation. Cells were further cultured in complete RPMI medium supplemented with recombinant human IL-2 (100 U/ml). In some experiments, both polyclonal and OT-I cells were magnetically sorted as above, activated on tissue culture dishes coated with 1 µg/ml anti-CD3 (clone 145-2C11) and 3 µg/ml anti-CD28 (clone 37.51), both from BioLegend and further cultured as above. Finally, cultured cells were washed twice in PBS and injected i.v. or intra-tumorally to recipient mice.

Fluorescence-based in vitro killing assay

Fluorescent target cells were plated for 4 h and then incubated for 4, 12, or 24 h with in vitro-generated OT-I CTLs at effector-to-target ratios ranging from 1:2 to 8:1. Loss of the fluorescent content was used to determine target cell death [26]. After incubation, non-adherent CTLs and dead target cells were washed away with PBS free of Ca^{++} and Mg^{++}. The fluorescence of the remaining live target cells was quantified using a Typhoon-9410 laser flatbed scanner (GE healthcare). Fluorescence reading was focused 3 µm above the plate surface. The percentage of specific lysis was calculated as $100 \times (C - X)/C$, where *C* is fluorescence in the CTL-free condition and *X* is fluorescence in the presence of CTLs.

Preparation of mice for intravital imaging

Mice with tumors ranging between 16 and 36 mm^2 in size were anesthetized with 100 mg/kg ketamine + 15 mg/kg xylazine + 2.5 mg/kg acepromazine, supplemented hourly with half this dose. Mice were placed on a warmed stage and kept at a core temperature of 37 °C. A skin flap was separated from the abdominal muscle to expose the intradermal tumor which was then covered with a glass-bottom imaging chamber. For vascular imaging, mice were retro-orbitally injected with 2.5 µl of 2 µM Q-tracker 655 quantum dots (Life Science Technologies).

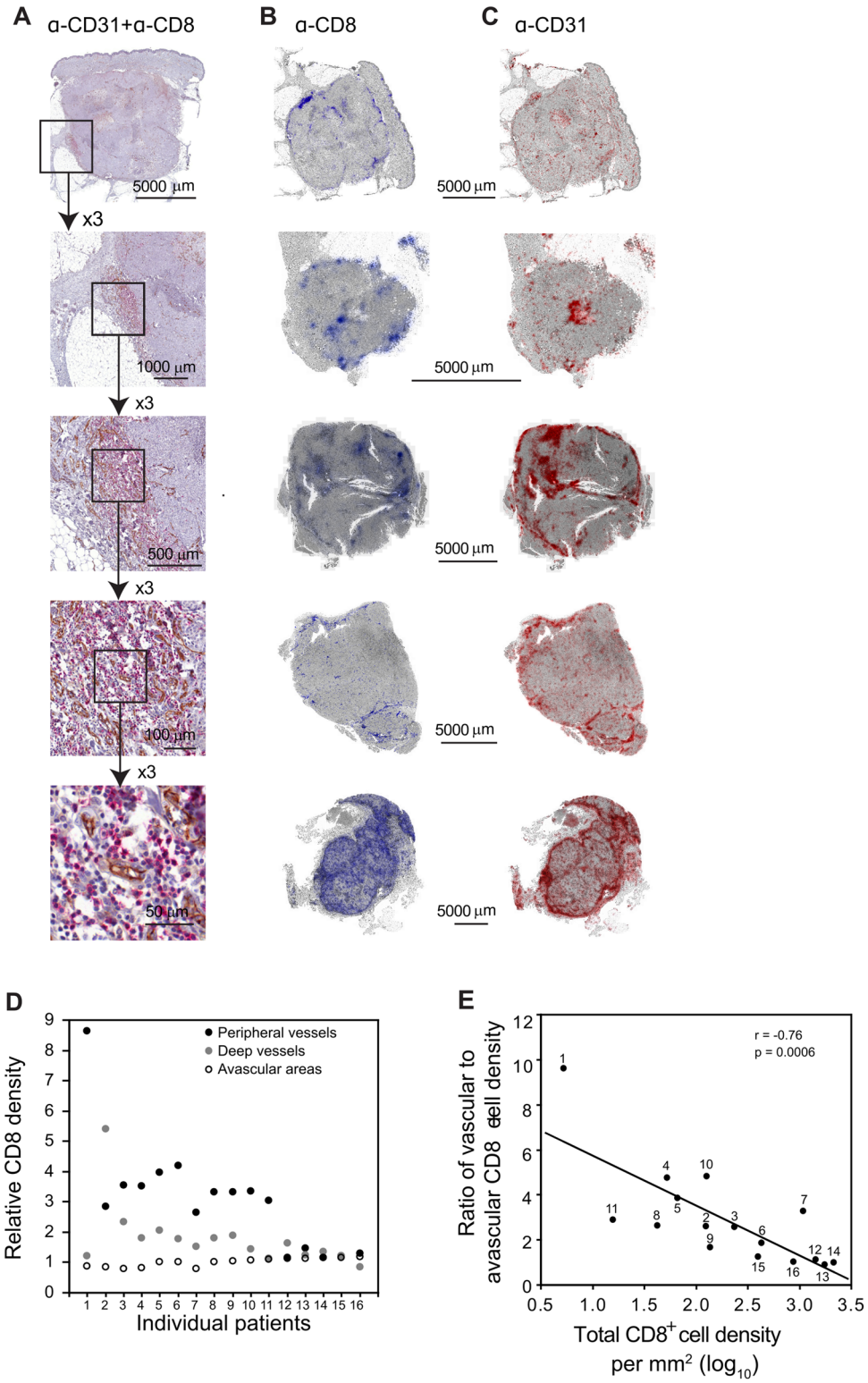

Fig. 1 $CD8^+$ cells in melanoma patients aggregate around peripheral blood vessels. **a** Immunohistochemical sections of a human melanoma metastasis shown at increasing magnification. Clusters of pink $CD8^+$ cells (mostly T cells) are enriched in brown $CD31^+$ cells (predominantly blood endothelial cells). **b**, **c** After staining, complete sections were scanned at high resolution, $CD8^+$ cells and blood vessels were automatically identified using color deconvolution, and their location was recorded (Figure S1). Shown are density maps of blood vessels (red) and $CD8^+$ cells (blue) from five individuals, demonstrating co-localization. **d** $CD8^+$ cells aggregated preferentially around peripheral blood vessels: comparison of relative $CD8^+$ cell densities around peripheral vessels, deep vessels and in avascular areas (see "Materials and methods" and Fig. S1). Individual patients are shown. $CD8^+$ cell density in vascular areas was three times higher than in avascular areas ($p < 0.03$), whereas cell density around peripheral vessels was more than two times higher than around deep vessels ($p < 0.04$), see also Table S1. **e** The degree of tumor infiltration by $CD8^+$ cells is inversely related to the homogeneity of their distribution. The ratio of $CD8^+$ cell densities in vascular and avascular areas is depicted against the log of total $CD8^+$ cell density in individual tumors. There was a significant ($p = 0.006$) inverse correlation ($r = -0.76$) between vascular preference and the degree of infiltration. Numbers indicate patient identity as in **d**

Live 2-photon microscopy of melanoma tumors

We used an Ultima™ Multiphoton Microscope (Prairie Technologies) incorporating a pulsed Mai Tai™ Ti–sapphire laser (Newport Corp., CA). Four optical channels were used: 470–510 nm to detect collagen fibers and CFP; 500–550 nm to detect GFP and CFP; 570–620 nm to detect tdTomato; and 620–680 nm to detect 655 quantum dots. Thus, CFP^+ cells were detected in the first two channels. The laser was tuned to 890–910 nm to simultaneously excite CFP, GFP,

tdTomato, and quantum dots. A water-immersed 20X (NA 0.95) or 40X objective (NA 0.8) from Olympus was used. The second harmonic signal produced by collagen fibers was detected with the laser tuned to 910 nm. To create a time-lapse sequence, a 150-µm-thick volume of the tumor was typically scanned at 5–6 µm Z-steps every 50 or 100 s. To assess the effect of blood flow on CTL motility in tumors, mice were imaged for 30 min to determine baseline motility. All visible blood vessels feeding into the tumors were then cauterized, resulting in a marked slowdown of blood flow. Imaging was resumed immediately for additional 30 min.

Assessing hypoxia in mouse melanoma samples

Tumor-bearing mice were injected with 60 mg/kg pimonidazole (1-[(2-hydroxy-3-piperdinyl)propyl]-2-nitroimidazole hydrochloride) (hypoxyprobe). Thirty minutes later, mice were sacrificed and tumors were excised and fixed with 2% paraformaldehyde. Fixed subcutaneous tumors were embedded in paraffin and sectioned at 4 µm. Following rehydration in xylene, 70%, 90%, and 100% ethanol, slides underwent peroxidase blocking with 3% hydrogen peroxidase, and then boiled in 0.1 M citric acid for antigen retrieval. Sequential slides were blocked by BSA and incubated with 1:100 rabbit anti mouse GFP or 1:100 PAb2627 rabbit antisera containing hypoxyprobe mAb. Following incubation with primary antibodies, slides were incubated with biotinylated anti-rat or anti-rabbit antibodies. Detection was performed with streptavidin-conjugated DAB antibodies. After staining, slides were dehydrated in 70%, 90%, and 100% ethanol for 1 min each, cleared in xylene for 1 min, and mounted with Entellan.

To quantify cell densities, consecutive GFP, and hypoxyprobe-stained tumor sections were digitally aligned, the tumor was demarcated for hypoxic and normoxic areas based on hypoxyprobe staining, the number GFP^+ cells in each area was calculated by dividing the GFP^+ area by the average cell area, and their density was determined by dividing this number by the total relevant area.

In vitro live cell imaging

For the in vitro migration assay, OT-I CTLs were re-suspended in complete RPMI medium at 2.5×10^5 cells/ml and seeded on a 35 mm glass-bottom dish (MatTek corporation) coated with 1 mg/ml fibronectin. Cellular motility was visualized in regular medium, medium with 1.5 µM carbonyl cyanide-4-(trifluoromethoxy) phenylhydrazone (FCCP), or oxygen-depleted medium (cultured overnight and maintained through the experiment at 1% oxygen, 5% CO_2, and 94% nitrogen). Images were taken at 15 s intervals using differential interference contrast (DIC) microscopy and fluorescence microscopy on a Nikon Eclipse T*i* inverted spinning-disk confocal microscope with a 20X air objective and acquired using the Andor iQ software.

Quantification of cell density and motility

The movement and distribution of CTLs were analyzed using the Volocity® software (PrekinElmer). Average velocities along the cell tracks were used to calculate three-dimensional velocity in vivo or two-dimensional velocity in vitro. The densities of cells in the perivascular and avascular tumor areas were calculated by automatically counting cells located within or beyond 50 µm of blood vessels and dividing these figures by the respective areas.

Statistical analysis

Tumor growth curves were compared based on the mean slope starting at the first day after CTL transfer [27]. Simple comparisons were made using a two-tailed Student's *t* test and multiple comparisons were performed by one-way ANOVA followed by the Bonferroni post hoc tests for multiple planned comparisons or the Dunnett test in comparisons with a control condition. Significance was set at $p < 0.05$. Data in figures are shown as mean ± SEM.

Results

In human melanoma samples, $CD8^+$ cells concentrate around peripheral blood vessels

The previous research has anecdotally observed that the pattern of infiltration of CD8 T cells into melanoma tumors can be heterogeneous. We quantified this phenomenon in melanoma tumor sections. We examined 16 subcutaneous metastases from stage-IV patients. Full cross sections were co-stained for CD8 and CD31 to show the relative distribution of endogenous $CD8^+$ cells and blood vessels (Fig. 1a) and then scanned and analyzed. Although some human NK cells (but not DCs) dimly express CD8 [28], they are typically outnumbered more than 30-fold by CD8 T cells [12], and thus, the latter cells likely represent the bulk of our enumerated population.

Tumors were variably infiltrated by $CD8^+$ cells that exhibited lymphocyte morphology, producing cell densities ranging from 5 to ~2150 cells/mm^2 (Fig. 1b, Table S1). Unless $CD8^+$ cell infiltration was massive, the cells distributed unevenly, creating discrete infiltration foci within tumors. $CD8^+$ cell infiltration seemed to occur mostly around $CD31^+$ blood vessels, particularly peripheral ones (Fig. 1c).

We used an automated procedure (Fig. S1) to quantify this phenomenon (Fig. 1d). The density of $CD8^+$ cells in vascular areas was three times higher than in avascular areas,

while cell density around peripheral vessels (defined as in Fig. S1f) was more than two times higher than around deep vessels. Noticeably, in tumors invaded by more $CD8^+$ cells, cellular distribution was more homogenous, as the degree of infiltration was inversely correlated with vascular preference (Fig. 1e). Perhaps, $CD8^+$ T begin to breach the perivascular confinement only when they accumulate in the tumor in larger numbers.

Establishing a model for intratumoral CTL killing

We established a murine model based on in vitro-activated fluorescent OT-I CTLs that eliminate fluorescent B16-OVA tumor cells. From the B16a tumor line, which expresses low levels of melanin [25], we produced lines transgenic for OVA-GFP or OVA-tdTomato as well as control lines that express the fluorescent reporters alone. As expected, OVA-expressing lines were specifically killed by OT-I CTLs in vitro (Fig. S2a), and formed tumors when injected intradermally. Such tumors could be rejected following adoptive transfer of OT-I CTLs (Fig. S2b). To better mimic real-life therapeutic situations and to challenge the CTLs with non-trivial rejection conditions, reasonable numbers of CTLs were transferred only after the tumors had already been well-established. This would prevent a ceiling effect and allow detection of subtler differences in CTL efficiency.

CTLs enter the tumor through specific blood vessels, accumulate in perivascular areas, and clear them from tumor cells

Intravital two-photon microscopy allowed us to follow the motility of CTLs and their interaction with tumor cells in relation to blood vessels. Mice were intradermally inoculated with 2×10^6 B16-OVA-GFP tumor cells in the flank, intravenously injected with 2×10^7 CFP^+ OT-I CTLs 7 days later and imaged 2 days later. A pattern similar to human melanoma tumors could be observed (Fig. 2a). Although the infiltration of CTLs was sizeable, they clustered mainly around blood vessels, yielding a threefold higher density of CTLs in the perivascular areas (defined as 50 µm around blood vessels) than in avascular areas (1644 vs. 528 cells/mm^2). The distribution of tumor cells, in contrast, was homogenous (369 vs. 374 cells/mm^2). As a result, the median distance of OT-I CTLs to the nearest blood vessel was half that of B16-OVA tumor cells (18.27 vs. 36.04 µm) (Fig. 2b).

CTLs could be watched extravasating out of peripheral blood vessels (Movie S1) and forming perivascular infiltrates consisting of motile cells (Movie S2). The density of CTLs varied considerably, with specific (likely inflamed) vessels attracting the majority of cells (Fig. 2c). One day later, the initial infiltrates had merged to form larger perivascular swarms, whose local CTL densities reached 250,000 cells/mm^3 (Movie S3). Observing the margin of the CTL swarms, two areas could be discerned (Fig. 2d, Movie S4). In the perivascular area, CTLs were numerous and fewer tumor cells could be observed. At the margin of this area, CTLs could be detected clustering around dying tumor cells. In the avascular area, fewer CTLs were present and tumor cells appeared intact. This observation suggests that large numbers of T cells need to directly attack B16 cells to kill them, a situation that does not occur in avascular tumor areas.

For efficient tumor clearance, multiple CTLs need to directly contact Ag-specific target cells

To assess whether perivascular CTLs' distribution actually hinders tumor rejection, we followed the behavior and activity of CTLs as they traveled through the tumor. Less than 10% of the analyzed CTLs formed stable (longer than 4 min) conjugates with tumor cells. The killing of target cells (Fig. 3a, Movies S4–S6) was recorded based on membrane blebbing, consistent with apoptosis (85–90% of events), or sudden loss of fluorescent cell content, consistent with lysis (10–15%). In the latter case, the exposed nucleus could be visualized with systemically injected propidium iodide (P.I.). Whereas 1:1 CTL:tumor cell conjugates rarely led to target cell elimination, higher ratios increased the efficiently, and when 5 or more CTLs engaged a single target, it was killed within an hour in more than a third of the cases (Fig. 3b).

To assess which molecular mechanism of target cell lysis was dominant in our tumor model, we used C57BL/6 mice deficient in FasL or perforin, two effector molecules pivotal in T-cell cytotoxicity [6, 7]. Identically cultured CTLs isolated from OT-I mice crossed with C57BL/6 mice deficient in FasL or perforin were used in tumor rejection assays (Fig. 3c). Whereas $FasL^{-/-}$ OT-I CTLs rejected tumors as efficiently as wild-type OT-I CTLs, $perforin^{-/-}$ OT-I CTLs performed poorly.

To test whether CTLs can indirectly eliminate bystander tumor cells in an Ag-independent manner, mice were inoculated with a mixture of differentially labeled OVA^+ and OVA^- B16 cells. The two cell populations proliferated similarly, maintained the original injection ratios, and formed thoroughly admixed tumors (Fig. 3d). When mice were treated with OT-I CTLs, in perivascular areas, infiltrated by OT-I CTLs, OVA^- cells remained intact, while OVA^+ cells were no longer apparent (Fig. 3e), in non-infiltrated areas, the ratio of OVA^+ and OVA^- target cells stayed constant, providing an internal control. Taken together, these results suggest that efficient killing requires TCR-mediated conjugates leading to perforin and granzyme release by several CTLs.

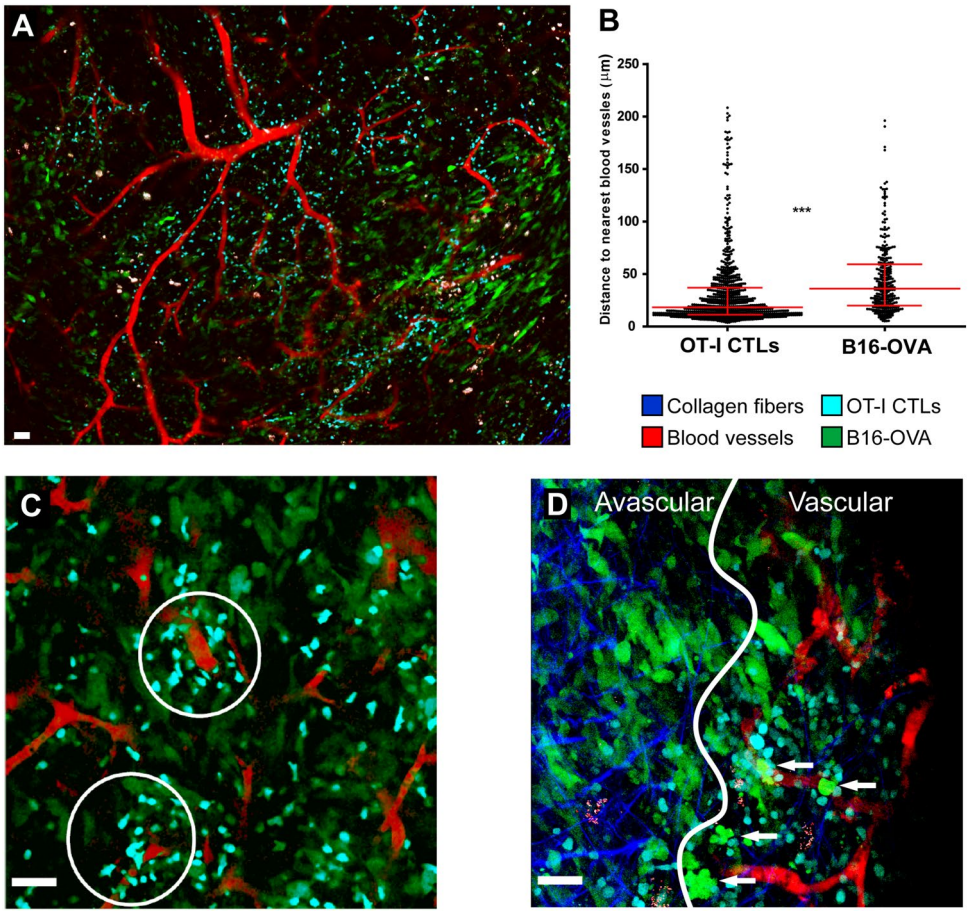

Fig. 2 CTLs enter the mouse tumors through specific blood vessels, cluster around target tumor cells and clear consecutive areas of the tumor. In vitro-activated OT-I CFP^+ CTLs were adoptively transferred to C57BL/6 mice-bearing B16-OVA-GFP tumors and were imaged by intravital two-photon microscopy following i.v. injection of red Quantum dots. Size bar = 50 µm. **a** Composite view of intratumoral CTL dissemination in relation to blood vessels. Two days following transfer, CTL distribution was heterogeneous and most cells concentrated around blood vessels. **b** Distances of CTLs ($n = 842$) and B16-Ova tumor cells ($n = 327$) to the nearest blood vessels were measured. CTLs were situated significantly closer to blood vessels than tumor cells ($p < 0.0001$). Shown are individual cell distances with the median and interquartile range shown in red. Data are representative of more than ten experiments. **c** More detailed view of CTL distribution. Perivascular infiltrates of CTLs appear around selected blood vessels (circled), likely representing their point of entry into the tumor. Size bar = 50 µm. **d** CTL activity was examined 3 days following transfer at the margin of vascularized areas. In the perivascular area (up to 50 µm from vessels) CTLs outnumbered tumor cells more than 2–1 and sometimes engaged in lytic conjugates (arrows), whereas the avascular area contained fewer CTLs and abounded with intact tumor cells (at ~ 1–2 ratio). Size bar = 50 µm

CTL motility depends on blood flow in vivo and on oxygen in vitro

To understand why CTLs infiltrate avascular areas poorly, we tracked CTLs experiencing different vascular densities. To control for experimental variability, we examined relative, rather than absolute, cell speeds in differently vascularized areas within the same imaging fields (Fig. 4a, Movie S7). Mapping cell velocities (Fig. 4b) revealed that they gradually subsided away from blood vessels. At distances greater than 50 µm, velocities were significantly lower than closer to blood vessels (Fig. 4c), and CTLs became scarcer.

We initially hypothesized that CTLs arrested due to the "TCR stop signal", as they interact with target cells [29]. Presumably, as CTLs enter through blood vessels, they clear away the first tumor cells they encounter, leaving them free to move in areas around the vessels through which they entered. Once they travel further into the tumor, they reencounter fresh tumor cells and stop to interact with them.

To test this hypothesis, we conducted two experiments: first, we co-injected the mice intravenously with OT-I and polyclonal CTLs (identically activated with anti-CD3 and anti-CD28) (Fig. 4d, Movie S8). Regardless of antigen specificity, both CTL types slowed down as they moved away from blood vessels (Fig. 4e, f).

Second, we checked the pattern of OT-I CTL infiltration and their motility when injected directly into the tumor, rather than intravenously. One day following intratumoral

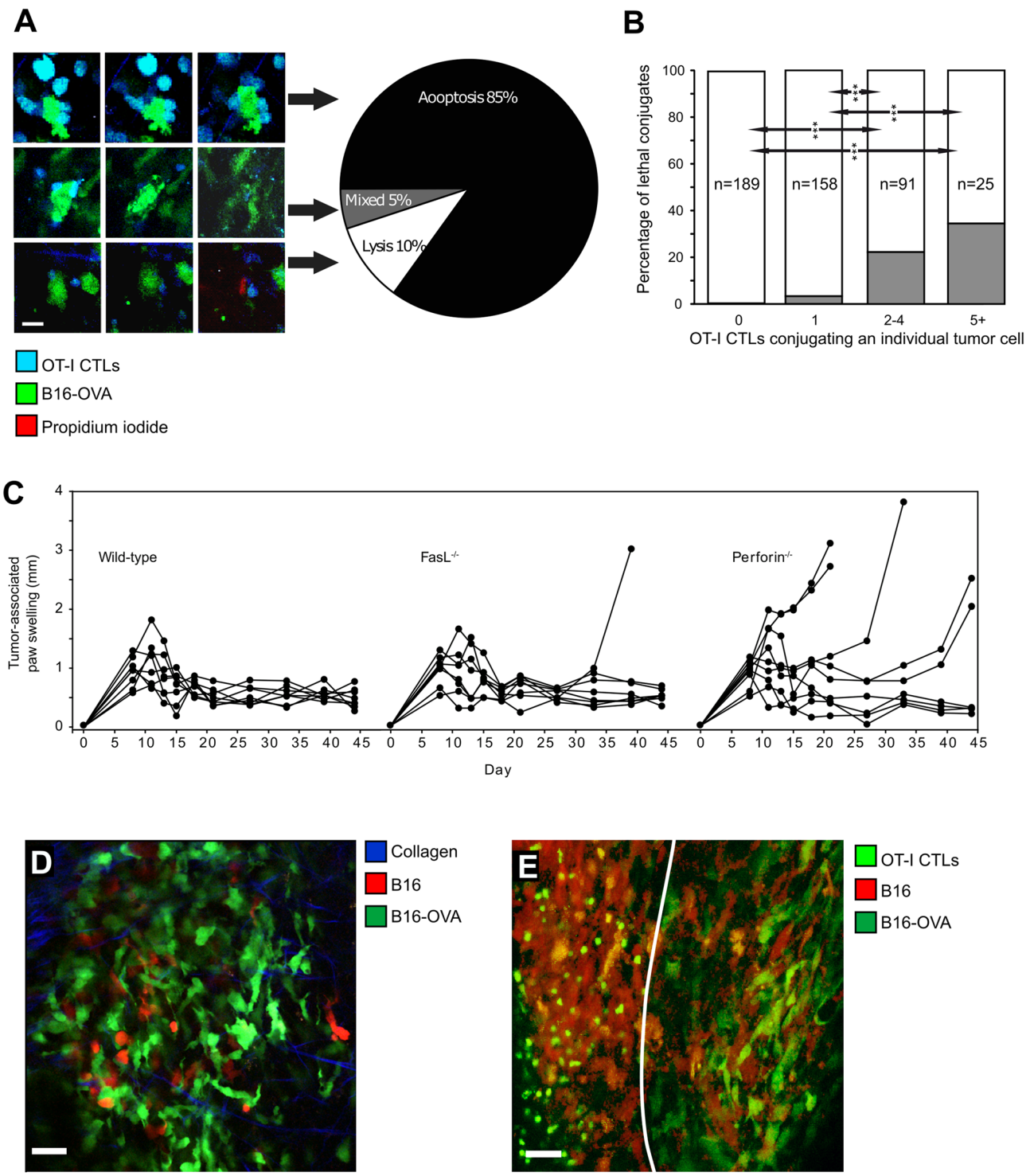

injection of 5×10^6 CTLs, they were observed congregating around intratumoral blood vessels (Fig. 4g), resulting in ~threefold higher CTL density in perivascular areas, where they exhibited vigorous motility (Movie S9). In areas farther away from the vessels, the cells slowed down and thinned out. Taken together, these experiments suggest that arrest due to TCR engagement is not a critical factor in CTL distribution.

An alternative hypothesis would suggest that CTLs rely on oxygen originating from blood vessels for optimal motility. This suggestion was supported by the effects of blood flow on CTL motility. We were following CTL motility in a tumor when a small capillary surrounded by CTLs became

◂**Fig. 3** CTL killing of tumor cells is contact- and antigen dependent. C57BL/6 mice-bearing B16-OVA-GFP tumors were injected with 2×10^7 in vitro-activated CFP$^+$ OT-I CTLs and imaged 2 days later by intravital 2-photon microscopy. ($n=34$ cells). **a** Tumor cell death most often took the form of apoptosis, indicated by membrane blebbing (top). Less often lytic death occurred, as indicated by abrupt loss of cytoplasmic GFP and exposure of the nucleus (bottom). Rarely, both processes occurred simultaneously (middle row). Loss of membrane integrity is revealed by P.I. staining. Size bar = 10 µm. **b** Rate per hour of tumor cell lysis increased with the number of CTLs engaging the target cell. **c** C57BL/6 mice were inoculated with B16-OVA tumor cells in their footpad and, 8 days later, were transferred with 5×10^6 in vitro-activated OT-I CTLs from either C57BL/6, FasL$^{-/-}$ or perforin$^{-/-}$ mice and were followed for tumor progression. Perforin$^{-/-}$ CTLs, but not FasL$^{-/-}$ CTLs rejected the tumor significantly less efficiently than wild-type CTLs ($p=0.04$, $n=8$ per group). **d** To test whether CTLs can indirectly eliminate bystander tumor cells in an Ag-independent manner, mice were injected with a mixture of OVA$^+$ GFP$^+$ B16 cells (green) and OVA$^-$ tdTomato$^+$ (red) B16 cells. Co-injection of a 2:1 mixture resulted in homogenously mixed tumors consisting of a similar proportion of cells (109:46 in this field). Data representative of five experiments. Size bar = 50 µm. **e** Mice inoculated with a tumor consisting of OVA$^+$ (green) and OVA$^-$ (red) B16 cells at a 1:1 ratio were treated with CTLs. In an un-infiltrated area (right), both OVA$^+$ GFP$^+$ and OVA$^-$ tdTomato$^+$ cells remained intact (53:51 in the demarcated area). In a highly infiltrated area (left), OVA$^+$ cells were all specifically eliminated, while 49 OVA$^-$ cells were spared. This result is inconsistent with efficient bystander killing in this model (data representative of 20 experiments). Size bar = 50 µm

spontaneously occluded (Fig. 5a, b, Movie S10). Within less than 100 s of occlusion, adjacent CTLs came to a complete arrest and rounded up; when blood flow spontaneously resumed, CTLs rapidly elongated and began to migrate. This rapid and reversible arrest suggests that CTLs respond to low oxygen levels rather than slow down because of nutritional deficits or accumulation of toxic metabolites. To verify this incidental finding, we cauterized blood vessels leading to the tumor, resulting in marked reduction in blood flow inside the tumor (Fig. 5c, Movie S11). As soon as blood flow was tampered with, CTLs rounded up ($p<0.0005$) and arrested.

These observations may have resulted from reduced oxygen around the blood vessels or from decreased flow of interstitial fluid near the vessel affecting mechanosensitive pathways. To directly test whether CTL motility depends on oxygen and on oxidative phosphorylation, CTL migration was examined in vitro (Fig. 5d, Movie S12). Upon depletion of oxygen, the cells rounded up and their crawling velocities dropped significantly. Inhibition of oxidative phosphorylation using the mitochondrial uncoupler FCCP had a similar affect without compromising cell viability (Fig. S3).

It has been reported that CTLs avoid hypoxic tumor areas [18]. To examine whether this applies to our tumor model, we immunohistochemically stained GFP$^-$ B16 OVA$^+$ tumors for tissue hypoxia (using pimonidazole adduct staining, Fig. S4a) and for transferred OT-I GFP$^+$ CTLs (using anti-GFP, Fig. S4b). As with CD8$^+$ cells in clinical samples, CTLs mostly localized to the tumor periphery and could be noticed around blood vessels. Comparing the patterns of CTL distribution and hypoxia, we observed mostly non-overlapping localization (Fig. S4c) and the density of CTLs in perivascular areas was 62% higher than in non-vascularized ones (2670 vs. 1650 cells/mm^2).

Discussion

To efficiently eliminate the tumor mass, CD8 T cells, whether endogenous or transferred, must disseminate in the tumor and physically contact their targets. We showed here in melanoma patients that, in most cases, the CD8$^+$ cells remain in perivascular areas, a pattern that likely leads to incomplete tumor rejection. In agreement with the previous studies in mice [22], for unknown reasons, CD8$^+$ cells accumulated preferably around peripheral, rather than deep vessels. Future studies could gain further insight on the CTLs located at different tumor areas by profiling their activation, proliferation, and exhaustion markers.

Modeling this phenomenon in mice, we showed that a large number of T cells need to contact their targets and eliminate them using antigen-dependent and perforin-mediated cytotoxicity. Tumor clearance is inefficient, as CTLs slow down away from blood vessels and sparsely penetrate hypoxic areas of the tumor.

Specifically, at early phases of infiltration, only 10% CTLs formed stable conjugates with tumor cells. Most of these conjugates consisted of one CTL and one target cell, and only 3% of them resulted in target cell death. The fact that CTLs proved inefficient killers is perhaps not surprising. Melanoma cells, B16 in particular, are resistant to cytolysis [30]. They express low levels of MHC-I [31], resist granzyme-mediated lysis [32], and exhibit multiple defects in the signaling of death receptors to TNF, FasL, and TRAIL, resulting from altered genomic, transcriptional, and post-translational regulation [33]. Similarly, using several tumor models in vivo, various imaging studies observed CTL arrest in contact with tumor cells and gross tumor rejection, but did not report any observations of killing events [20, 22, 34, 35]. Even when killing events were reported [21], their frequency was very low—only 13 killing events observed following 129 conjugates between CTLs and EG7 thymoma cells. Similarly, we observed only 34 unmistakable killing events in many hours of observation. We may have underestimated, though, the number of such events, as we relied on late morphological signs of cell death (blebbing, loss of GFP content, and exposure of nucleic acid) rather than molecular signatures.

We suggest that CTLs can combine forces and overcome tumor resistance by attacking a single tumor cell simultaneously or in short succession, resulting in several-fold higher

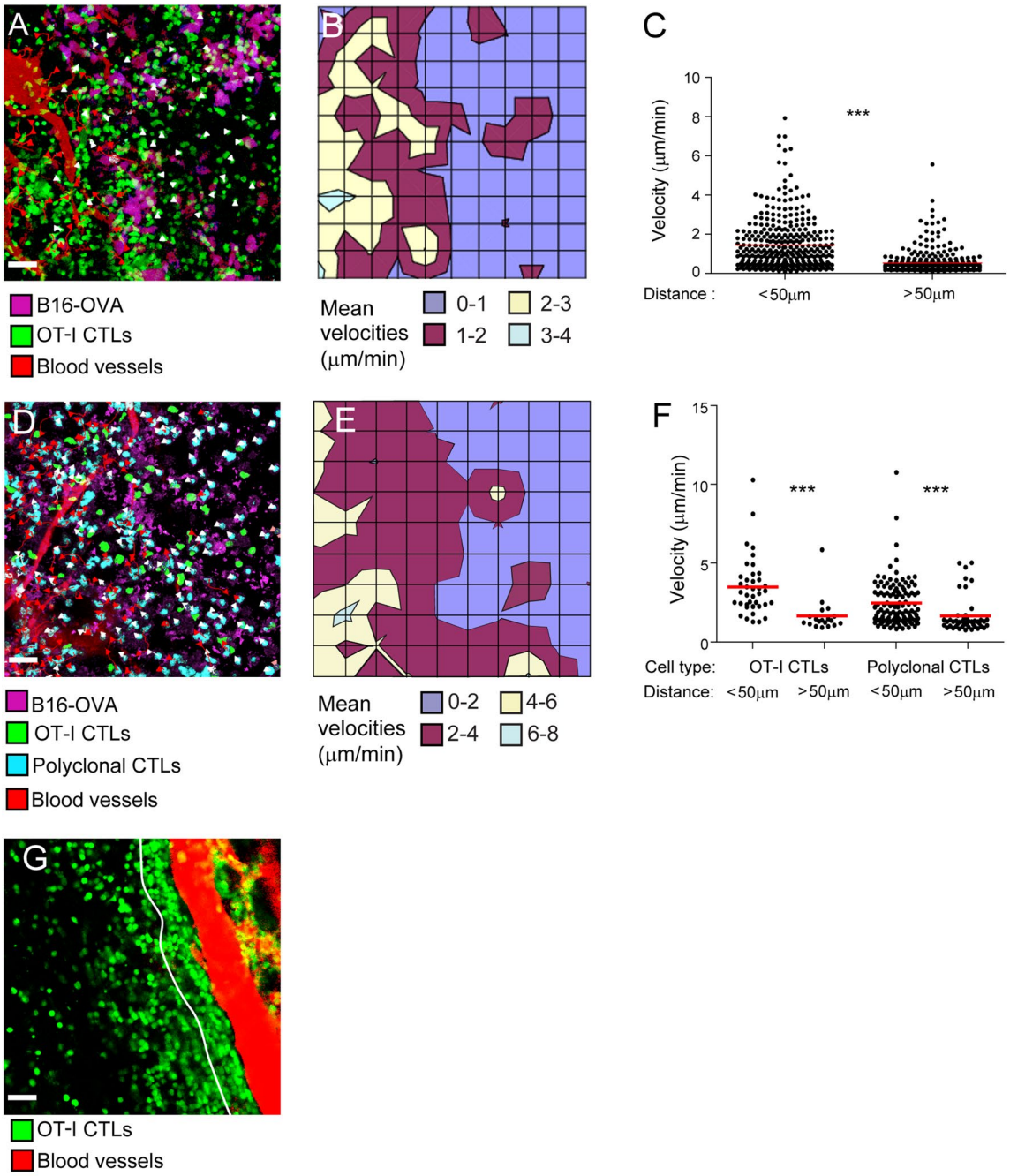

Fig. 4 CTLs decelerate as they move away from blood vessels. **a–c** Mice-bearing B16-OVA-tdTomato tumors (purple cells) were treated with 2×10^7 in vitro-activated OT-I CTLs (green). Two days later, their intratumoral motility was examined in relation to blood vessels (red). **a** In a partially vascularized tumor area, more sessile CTLs were observed in the avascular region on the right. Red tracks indicate CTL velocities exceeding 2.5 μm/min. White tracks indicates velocities below 2.5 μm/min. Size bar = 50 μm. **b** CTL velocity map of the imaging field in A indicates a gradual decline in migration velocities. **c** CTL velocities were higher close to blood vessels (< 50 μm) than farther away (> 50 μm) ($p < 0.0001$, $n = 668$ cells). Data were pooled form five experiments. **d–f** To test if CTL arrest resulted from interaction with antigen, in vitro-activated CFP^+ OT-I T cells (cyan) were co-injected with in vitro-activated GFP^+ polyclonal T cells (green). **d** In a partially vascularized tumor area, more sessile CTLs were observed in the avascular region on the right. Red and white tracks indicate CTL velocities as above. Size bar = 50 μm. **e** Velocity map of polyclonal CTLs indicates a gradual decline in their velocities. **f** ANOVA indicated that both cell types moved faster closer to blood vessels ($p < 0.0001$, $n = 255$) and were similarly affected, as no significant statistical interaction was observed ($p = 0.97$). Baseline speeds are non-zero due to imaging field drift. Data representative of more than five experiments. **g** When in vitro-activated CTLs were injected directly into the tumor, they congregated around blood vessels, resulting, in this field, in a 2.8-fold higher CTL density in the perivascular (< 50 μm) than in the avascular area (7080 vs. 2515 cells/mm^2). Based on analysis of 714 cells. Data representative of four experiments. Size bar = 50 μm

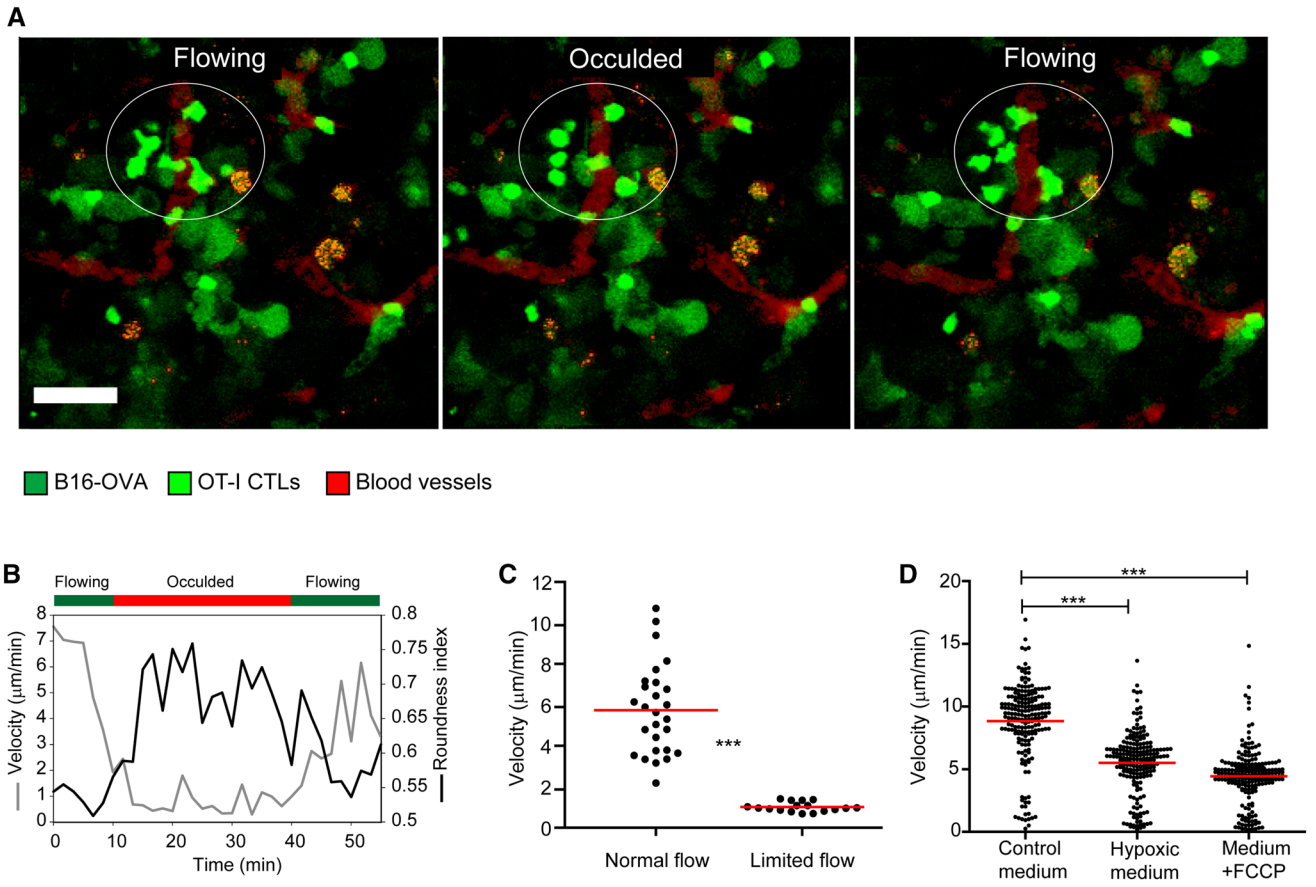

Fig. 5 CTLs arrest upon disruption of blood flow or hypoxia. **a** Successive images of the motility of CTLs (activated as above) around transiently occluded capillaries. When blood was flowing (left), CTLs were motile as indicated by their amoeboid shape. Immediately after capillary occlusion (middle), CTLs arrested and rounded up. Immediately after blood flow resumed (right), CTL regained their amoeboid shape, reflecting normal migration. Size bar = 50 μm. **b** CTL velocity and roundness over time as the flowing status of the capillary changed in **a**. **c** CTLs arrest upon deliberate interruption of blood flow to the tumor ($p < 0.0001$, data representative of three experiments). **d** OT-I CTLs were plated on fibronectin-coated glass-bottom plates and were followed using a spinning disk confocal microscope for 20 min. Compared to control medium, CTL velocities dropped in oxygen-depleted (hypoxic) medium ($p < 0.0001$) and in the presence of 1.5 μM FCCP—a mitochondrial uncoupler that inhibits oxidative phosphorylation ($p < 0.0001$). Data are representative of four experiments

success rates. Inside CTL swarms, local effector-to-target ratios are high, and such conditions prevail. This in vivo observation corroborates in vitro findings [30], showing that CTLs must deliver multiple hits to annihilate B16 melanoma cells.

A recent in vivo imaging study [36] that followed elimination of virally infected target cells, observed similar CTL behavior. The authors demonstrated that killing rates increased non-linearly when multiple CTLs contacted the infected cells and concluded that CTLs cooperate to maximize killing. Such findings do not necessarily imply communication or synergy between CTLs. An equally valid explanation would suggest that a threshold concentration of effector molecules needs to be reached before the target cell succumbs to cytolysis.

The need for multiple CTLs for efficient killing is compounded by the lack of apparent bystander target cell killing in the model we used: antigen-negative target cells could survive in CTL-infiltrated areas cleared of antigen-expressing cells, suggesting that effector–target cell contact is essential. Correspondingly, perforin$^{-/-}$ OT-I CTLs rejected the tumors less efficiently than wild-type OT-I CTLs. Such strict antigen dependence is in agreement with previous imaging studies [21] but not with others [10], suggesting that the extent of bystander killing may depend on the exact tumor model used.

To reliably capture enough lytic immunological synapses, we resorted to using a model based on high numbers of OT-I CTLs recognizing the exogenous OVA antigen with high affinity. We expect that naturally occurring tumor antigens, which typically bind TCRs with lower affinities, would elicit lower killing efficiency. Thus, in the clinical setting, an additive effect of poor infiltration due to hypoxia and inefficient killing due to low affinity could result in tumor persistence.

The main conclusion of this study, albeit based on a single tumor model and on specific conditions in which the anti-tumor response is partial is this: anti-tumor CTL activity is limited by the perivascular distribution of CTLs, likely promoted by hypoxia in deeper tumor areas. Several lines of evidence converge to support this notion: (1) the speed of CTLs (both Ag-specific and non-specific) declined as they moved away from blood vessels; (2) when injected intratumorally, CTLs concentrated around blood vessels, where they migrated vigorously; (3) CTLs arrested upon deliberate or sporadic occlusion of blood vessels and motility resumed when blood flow was renewed; (4) T cells accumulated in normoxic areas and avoided hypoxic ones; and (5) the in vitro motility of CTLs declined in anaerobic conditions or when oxidative phosphorylation in mitochondria was blocked.

Echoing our findings, recent work [18] demonstrated that T cells avoid hypoxic tumor areas and that prolonged respiratory hyperoxia (with 60% oxygen) induces accumulation of CD8 T cells in tumors and promotes the T-cell-dependent regression of metastasis. Surprisingly, a recent paper [37] established that sensing high oxygen levels inhibits the activity of endogenous T cells against B16 tumors. Importantly, effects were seen within B16 lung metastases, where oxygen levels are high, but not in subcutaneous tumors. Culturing TCR-transgenic CD4 T cells at hypoxia-inducing conditions greatly improved their ability to reject s.c. tumors upon adoptive transfer. Possibly, this treatment acclimatized the cells to the hypoxic conditions rife within s.c. tumors. More insight into this question could be gained in the future by comparing the distribution and motility of intratumoral CTLs in conditions leading to tumor rejection or not.

The molecular mechanisms through which hypoxia impairs CTL motility remain unknown. Judging on how fast perivascular CTLs respond to changes in blood flow, it is unlikely to depend on transcription (downstream of HIF-1, for instance) or energetic deficits. Instead, it might be mediated by oxygen sensors directly coupled to cytoskeletal machinery. Such biochemical pathways link prolyl hydroxylase domain-containing protein 2 (PHD2), Ras homolog gene family, member a (RhoA) and cofilin [38], as well as PHD3 and actin [39], affecting cell motility.

Other mechanisms may work in parallel to hypoxia to keep CTLs in the perivascular niche. Less glucose is probably available in avascular tumor areas. Although the effect of glucose availability on the motility of CTLs was not studied, it was recently shown to be critical for CTL activation, IFN-γ production, and tumor rejection [17, 40]. Another possibility is that hypoxia leads to accumulation of adenosine in avascular tumor areas, which in turn suppresses T-cell function, and perhaps their motility [18, 41]; lactic acid may play a similar role [42]. M2-like tumor-associated macrophages, which are attracted to hypoxic and necrotic areas in the tumor [43–45], may contribute to T-cell dysfunction in these areas. Moreover, chemokines secreted or immobilized in the perivascular area may attract CTLs to this particular region and promote their motility. Indeed, a study of primary central nervous system (CNS) lymphoma [46] identified clusters of CTLs around blood vessels and strongly suggested that the chemokines CXCL9 and CXCL12, produced by pericytes and macrophages, attracted these cells to the perivascular region. Finally, FasL, expressed on the vessels of several tumor types, may preferentially kill CTLs upon their entry to the tumor [47]. This finding, though, is unlikely to explain the phenomenon that we observed, as CTLs accumulated outside the vessels and were highly motile in this area, thus unlikely to be undergoing FAS-mediated death. Overall, several mechanisms may collude to keep CTLs next to blood vessels in tumors. Most, though, cannot explain the immediate arrest of CTLs when blood flow is compromised.

Bypassing the dependence of CTLs on oxygen can potentially improve immunotherapy. Several strategies could be attempted. Clinicians can try to normalize tumor vascularization through systemic treatment. Indeed, extensive work from the laboratory of Rakesh Jain has shown that achieving this goal with limited doses of anti-VEGF in mice can promote tumor rejection [48] and that clinical anti-angiogenic therapy, when effective, delays tumor development through normalization, rather than elimination of blood vessels [49]. Pursuing that notion, several groups have demonstrated that vascular normalization promotes T-cell-based anti-tumor immunity [50, 51] and can be used synergistically with immunotherapy in animal models [52–54].

An alternative approach would be to systemically increase the availability of oxygen. This may be achievable in patients using hyperbaric chambers or oxygen masks. Accordingly, as mentioned above, housing mice in hyperoxic chambers were shown to reduce hypoxic areas in metastases and primary tumors, induce the accumulation of tumor-infiltrating CTLs, and promote tumor regression [18].

The study by Clever et al. [37] portrayed a more complicated picture. The findings established that sensing high oxygen tension inhibited the anti-tumor activity of endogenous CD4 T cells within b16 lung metastases, but not subcutaneous tumors. Culturing TCR-transgenic CD4 T cells at hypoxia-inducing conditions greatly improved their ability to reject s.c. tumors upon adoptive transfer. It might have been the case that such treatment adapted the cells to the hypoxic conditions rife within s.c. tumors, but since this study focused on CD4 T-cell function, it cannot be directly compared to ours.

A final strategy would be to culture CTLs in conditions that favor their resistance to hypoxia. This approach would be relevant to adoptive immunotherapy with TILs, TCR- or CAR-transfected T cells, but not to therapies based on endogenous CTLs. The previous research has already shown

that CTLs can grow in low oxygen conditions and function in vitro [55, 56]. Our recent findings indicate that CTLs raised under hypoxic conditions produce more granzyme B and excel at killing melanoma cells in vitro and in vivo [57]. In vivo anti-tumor CTL function is obviously more complex than in vitro cytotoxicity. It requires, among other things, infiltration into tumors and migration within them. While naïve T cells may adapt to hypoxic conditions and function well, fully mature CTLs may lose this plasticity. In our experience, naïve T cells enter tumors very inefficiently. For these reasons, when considering cellular immunotherapy, effector T cells may need to be adapted in vitro to hypoxic conditions, so that they are ready to infiltrate the tumors and function fully upon transfer.

We conclude that in humans as in mice, $CD8^+$ T cells tend to concentrate near blood vessels in melanoma tumors. Our dynamic studies in mice suggest that the hypoxia experienced by these cells away from flowing blood vessels contributes to this phenomenon. Since tumor cells might use hypoxic areas in the tumors to escape CTL attack in immunotherapeutic contexts, better understanding of this phenomenon, and the ways to circumvent that it is pertinent.

Author contributions YM and TF performed the experiments and wrote the paper, AH and GS performed additional experiments, ZS assisted with analysis, and MK assisted with data visualization. CA and BS prepared clinical samples, IB and MJB provided these samples, and GS conceived and planned the project and helped writing the paper.

Funding Guy Shakhar and Tali Feferman were supported in this project by grants from the Israel Science Foundation (Grant 1735/15), the Israel Cancer Association (Grant no. 20170182), and from the German Cancer Research Center and the Israeli ministry of Science and Technology (DKFZ-MOST) (Grant no. GR2353) collaborative program.

Compliance with ethical standards

Conflict of interest The authors declare that they have no conflict of interest.

Ethical approval and ethical standards Experiments were approved by the institutional animal care and use committee and the Institutional Review Board at the Weizmann Institute of Science. Protocol number 40351217-2. We followed the guidelines for animal use in research in Israel and for the use of specimens of human origin.

Informed consent All patients signed a form consenting to the use of diagnostic samples taken from them for anonymous, non-commercial research purposes.

Animal source C57BL/6 mice were purchased from Harlan laboratories Ltd. All other mouse strains were purchased from the Jackson Laboratories and bred locally.

Cell line authentication Cells from the B16a melanoma line [25] were kindly provided by Prof. Bonnie Sloane at Wayne State University, Detroit, MI. Cells were periodically tested for the presence of mycoplasma and found clean. All lines were used within ten passages. Expression of OVA and fluorescent proteins after cell passages was confirmed by flow cytometry. All tumor lines grew rapidly in untreated immunocompetent syngeneic C57BL/6 mice and formed pigmented tumors typical of melanoma.

References

1. Vesely MD, Kershaw MH, Schreiber RD, Smyth MJ (2011) Natural innate and adaptive immunity to cancer. Annu Rev Immunol 29:235–271
2. Coulie PG, Van den Eynde BJ, van der Bruggen P, Boon T (2014) Tumour antigens recognized by T lymphocytes: at the core of cancer immunotherapy. Nat Rev Cancer 14:135–146
3. Angell H, Galon J (2013) From the immune contexture to the immunoscore: the role of prognostic and predictive immune markers in cancer. Curr Opin Immunol 25:261–267
4. Aerts JG, Hegmans JP (2013) Tumor-specific cytotoxic T cells are crucial for efficacy of immunomodulatory antibodies in patients with lung cancer. Cancer Res 73:2381–2388
5. Herbst RS, Soria J-C, Kowanetz M, Fine GD, Hamid O, Gordon MS et al (2014) Predictive correlates of response to the anti-PD-L1 antibody MPDL3280A in cancer patients. Nature 515:563–567
6. Trambas CM, Griffiths GM (2003) Delivering the kiss of death. Nat Immunol 4:399–403
7. Berke G (1995) The CTL's kiss of death. Cell 81:9–12
8. Voskoboinik I, Whisstock JC, Trapani JA (2015) Perforin and granzymes: function, dysfunction and human pathology. Nat Rev Immunol 15:388–400
9. Zhang B, Karrison T, Rowley DA, Schreiber H (2008) IFN-gamma- and TNF-dependent bystander eradication of antigen-loss variants in established mouse cancers. J Clin Investig 118:1398–1404
10. Schietinger A, Arina A, Liu RB, Wells S, Huang J, Engels B et al (2013) Longitudinal confocal microscopy imaging of solid tumor destruction following adoptive T cell transfer. Oncoimmunology. 2:e26677
11. Galon J, Costes A, Sanchez-Cabo F, Kirilovsky A, Mlecnik B, Lagorce-Pagès C et al (2006) Type, density, and location of immune cells within human colorectal tumors predict clinical outcome. Science 313:1960–1964
12. Erdag G, Schaefer JT, Smolkin ME, Deacon DH, Shea SM, Dengel LT et al (2012) Immunotype and immunohistologic characteristics of tumor-infiltrating immune cells are associated with clinical outcome in metastatic melanoma. Cancer Res 72:1070–1080
13. Kiss J, Timar J, Somlai B, Gilde K, Fejos Z, Gaudi I et al (2007) Association of microvessel density with infiltrating cells in human cutaneous malignant melanoma. Pathol Oncol Res 13:21–31
14. Brizel DM, Scully SP, Harrelson JM, Brizel M, Harrelson M, Layfield J et al (1996) Tumor oxygenation predicts for the likelihood of distant metastases in human soft tissue sarcoma. Cancer Res 56:941–943
15. Höckel M, Schlenger K, Aral B, Mitze M, Schaffer U, Vaupel P (1996) Association between tumor hypoxia and malignant progression in advanced cancer of the uterine cervix. Cancer Res 56:4509–4515
16. Huang JH, Cardenas-Navia LI, Caldwell CC, Plumb TJ, Radu CG, Rocha PN et al (2007) Requirements for T lymphocyte migration in explanted lymph nodes. J Immunol 178:7747–7755
17. Chang CH, Qiu J, O'Sullivan D, Buck MD, Noguchi T, Curtis JD et al (2015) Metabolic competition in the tumor microenvironment is a driver of cancer progression. Cell 162:1229–1241
18. Hatfield SM, Kjaergaard J, Lukashev D, Schreiber TH, Belikoff B, Abbott R et al (2015) Immunological mechanisms of the

antitumor effects of supplemental oxygenation. Sci Transl Med 7:1–12
19. Mempel TR, Bauer CA (2009) Intravital imaging of CD8+ T cell function in cancer. Clin Exp Metastasis 26:311–327
20. Broz ML, Binnewies M, Boldajipour B, Nelson AE, Pollack JL, Erle DJ et al (2014) Dissecting the tumor myeloid compartment reveals rare activating antigen-presenting cells critical for t cell immunity. Cancer Cell 26:638–652
21. Breart B, Lemaitre F, Celli S, Bousso P (2008) Two-photon imaging of intratumoral CD8+ T cell cytotoxic activity during adoptive T cell therapy in mice. J Clin Investig 118:1390–1397
22. Boissonnas A, Fetler L, Zeelenberg IS, Hugues S, Amigorena S (2007) In vivo imaging of cytotoxic T cell infiltration and elimination of a solid tumor. J Exp Med 204:345–356
23. Ruifrok AC, Johnston DA (2001) Quantification of histochemical staining by color deconvolution. Anal Quant Cytol Histol 23:291–299
24. Zangi L, Klionsky YZ, Yarimi L, Bachar-Lustig E, Eidelstein Y, Shezen E et al (2012) Deletion of cognate CD8 T cells by immature dendritic cells: a novel role for perforin, granzyme A, TREM-1, and TLR7. Blood 120:1647–1657
25. Crissman JD, Hatfield J, Schaldenbrand M, Sloane BF, Honn KV (1985) Arrest and extravasation of B16 amelanotic melanoma in murine lungs. A light and electron microscopic study. Lab Investig 53:470–478
26. Steff AM, Fortin M, Arguin C, Hugo P (2001) Detection of a decrease in green fluorescent protein fluorescence for the monitoring of cell death: an assay amenable to high-throughput screening technologies. Cytometry 45:237–243
27. Heitjan DF, Manni A, Santen RJ (1993) Statistical analysis of in vivo tumor growth experiments. Cancer Res 53:6042–6050
28. Perez OD, Mitchell D, Jager GC, Nolan GP (2004) LFA-1 signaling through p44/42 is coupled to perforin degranulation in CD56+ CD8+ natural killer cells. Blood 104:1083–1093
29. Dustin ML, Bromley SK, Kan ZY, Peterson DA, Unanue ER (1997) Antigen receptor engagement delivers a stop signal to migrating T lymphocytes. Proc Natl Acad Sci USA 94:3909–3913
30. Caramalho I, Faroudi M, Padovan E, Muller S, Valitutti S, Müller S (2009) Visualizing CTL/melanoma cell interactions: multiple hits must be delivered for tumour cell annihilation. J Cell Mol Med 13:3834–3846
31. Böhm W, Thoma S, Leithäuser F, Möller P, Schirmbeck R, Reimann J (1998) T cell-mediated, IFN-gamma-facilitated rejection of murine B16 melanomas. J Immunol 161:897–908
32. Khazen R, Puissegur M, Muller S, Valitutti S (2015) Dissecting early mechanisms of melanoma cell resistance to cytotoxic T lymphocyte attack (TUM10P.1025). J Immunol 194:211.6
33. Ivanov VN, Bhoumik A, Ronai Z (2003) Death receptors and melanoma resistance to apoptosis. Oncogene 22:3152–3161
34. Engelhardt JJ, Boldajipour B, Beemiller P, Pandurangi P, Sorensen C, Werb Z et al (2012) Marginating dendritic cells of the tumor microenvironment cross-present tumor antigens and stably engage tumor-specific T cells. Cancer Cell 21:402–417
35. Pentcheva-Hoang T, Simpson TR, Montalvo-Ortiz W, Allison JP (2014) Cytotoxic T lymphocyte antigen-4 (CTLA-4) blockade enhances anti-tumor immunity by stimulating melanoma-specific T cell motility. Cancer Immunol Res 4:970–980
36. Halle S, Keyser KA, Stahl FR, Busche A, Marquardt A, Zheng X et al (2016) In vivo killing capacity of cytotoxic T cells is limited and involves dynamic interactions and T cell cooperativity. Immunity 44:233–245
37. Clever D, Roychoudhuri R, Constantinides MG, Askenase MH, Sukumar M, Klebanoff CA et al (2016) Oxygen sensing by T cells establishes an immunologically tolerant metastatic niche. Cell 166(1117–1131):e14
38. Vogel S, Wottawa M, Farhat K, Zieseniss A, Schnelle M, Le-Huu S et al (2010) Prolyl hydroxylase domain (PHD) 2 affects cell migration and F-actin formation via RhoA/Rho-associated kinase-dependent cofilin phosphorylation. J Biol Chem 285:33756–33763
39. Luo W, Lin B, Wang Y, Zhong J, O'Meally R, Cole RN et al (2014) PHD3-mediated prolyl hydroxylation of nonmuscle actin impairs polymerization and cell motility. Mol Biol Cell 25:2788–2796
40. Ho PC, Bihuniak JD, MacIntyre AN, Staron M, Liu X, Amezquita R et al (2015) Phosphoenolpyruvate is a metabolic checkpoint of anti-tumor T cell responses. Cell 162:1217–1228
41. Hatfield SM, Kjaergaard J, Lukashev D, Belikoff B, Schreiber TH, Sethumadhavan S et al (2014) Systemic oxygenation weakens the hypoxia and hypoxia inducible factor 1α-dependent and extracellular adenosine-mediated tumor protection. J Mol Med (Berl) 92:1283–1292
42. Fischer K, Hoffmann P, Voelkl S, Meidenbauer N, Ammer J, Edinger M et al (2015) Inhibitory effect of tumor cell-derived lactic acid on human T cells. Blood 109:3812–3820
43. Van Overmeire E, Laoui D, Keirsse J, Van Ginderachter JA, Sarukhan A (2014) Mechanisms driving macrophage diversity and specialization in distinct tumor microenvironments and parallelisms with other tissues. Front Immunol 5:1–16
44. Casazza A, Laoui D, Wenes M, Rizzolio S, Bassani N, Mambretti M et al (2013) Impeding macrophage entry into hypoxic tumor areas by Sema3A/Nrp1 signaling blockade inhibits angiogenesis and restores antitumor immunity. Cancer Cell 24:695–709
45. Movahedi K, Laoui D, Gysemans C, Baeten M, Stangé G, Van Den Bossche J et al (2010) Different tumor microenvironments contain functionally distinct subsets of macrophages derived from Ly6C(high) monocytes. Cancer Res 70:5728–5739
46. Venetz D, Ponzoni M, Schiraldi M, Ferreri AJM, Bertoni F, Doglioni C et al (2010) Perivascular expression of CXCL9 and CXCL12 in primary central nervous system lymphoma: T-cell infiltration and positioning of malignant B cells. Int J Cancer 127:2300–2312
47. Hagemann IS, Lal P, Feldman MD, Benencia F (2014) Tumor endothelium FasL establishes a selective immune barrier promoting tolerance in tumors. Nat Med 20:607–615
48. Jain RK (2005) Normalization of tumor vasculature: an emerging concept in antiangiogenic therapy. Science (80-) 307:58–62
49. Sorensen AG, Emblem KE, Polaskova P, Jennings D, Kim H, Ancukiewicz M et al (2012) Increased survival of glioblastoma patients who respond to antiangiogenic therapy with elevated blood perfusion. Cancer Res 72:402–407
50. Li X, Kostareli E, Suffner J, Garbi N, Hämmerling GJ (2010) Efficient Treg depletion induces T-cell infiltration and rejection of large tumors. Eur J Immunol 40:3325–3335
51. Klug F, Prakash H, Huber PE, Seibel T, Bender N, Halama N et al (2013) Low-dose irradiation programs macrophage differentiation to an iNOS$^+$/M1 phenotype that orchestrates effective T cell immunotherapy. Cancer Cell 24:589–602
52. Manning EA, Ullman JG, Leatherman JM, Asquith JM, Hansen TR, Armstrong TD et al (2007) A vascular endothelial growth factor receptor-2 inhibitor enhances antitumor immunity through an immune-based mechanism. Clin Cancer Res 13:3951–3959
53. Hamzah J, Jugold M, Kiessling F, Rigby P, Manzur M, Marti HH et al (2008) Vascular normalization in Rgs5-deficient tumours promotes immune destruction. Nature 453:410–414
54. Huang Y, Yuan J, Righi E, Kamoun WS, Ancukiewicz M, Nezivar J et al (2012) Vascular normalizing doses of antiangiogenic treatment reprogram the immunosuppressive tumor microenvironment and enhance immunotherapy. Proc Natl Acad Sci USA 109:17561–17566
55. Caldwell CC, Kojima H, Lukashev D, Armstrong J, Farber M, Apasov SG et al (2001) Differential effects of physiologically

relevant hypoxic conditions on T lymphocyte development and effector functions. J Immunol 167:6140–6149
56. Nakagawa Y, Negishi Y, Shimizu M, Takahashi M, Ichikawa M, Takahashi H (2015) Effects of extracellular pH and hypoxia on the function and development of antigen-specific cytotoxic T lymphocytes. Immunol Lett 167:72–86
57. Gropper Y, Feferman T, Shalit T, Salame TM, Porat Z, Shakhar G (2017) Culturing CTLs under hypoxic conditions enhances their cytolysis and improves their anti-tumor function. Cell Rep 20:2547–2555